A New 3D Transient Thermoelectric Modelling Approach for an Aluminium Electrolysis Cell Considering Bath Chemistry Variations

Mehran Shahin[1], Martin Désilets[2], Marc LeBreux[3], Jean-François Bilodeau[4], Sébastien Guérard[5] and François Allard[6]
1. Ph.D. Candidate
2. Full Professor
Aluminium Research Centre-REGAL, Université de Sherbrooke, Sherbrooke, Canada
3. Research Assistant
Université de Sherbrooke, Sherbrooke, Canada
4. Senior Advisor R&D
5. R&D Scientist
Centre de recherche et développement Arvida, Rio Tinto Alcan, Saguenay, Canada
6. Assistant Professor
Aluminium Research Centre-REGAL, Centre Énergie, Matériaux et Télécommunications, Institut National de la Recherche Scientifique, Varennes, Canada
Corresponding author: mehran.shahin@usherbrooke.ca
https://doi.org/10.71659/icsoba2025-al088

Abstract

A novel approach is introduced to model the transient thermoelectric behaviour of an aluminium electrolysis cell using a 3D finite-element cell-slice model developed in Ansys and coupled with a Python submodel. This approach solves the model one timestep at a time, using nodal results from the previous step as initial conditions for the next. A moving interface between the molten liquids (electrolytic bath and aluminium) and the ledge was adopted, enabling variation of heat transfer over its height, thus representing the variation of the heat transfer coefficient with height by assigning different thermal contact conductances along the interface. Additionally, a simple yet extensible mass balance submodel was developed in Python and coupled with the finite-element model, accounting for the influence of bath melting/freezing and also the bath film (between the metal and ledge) on bath chemistry. A power modulation scenario with electrolyte freezing and melting periods was simulated using the coupled model, and results were compared to those obtained with a calibrated cell-slice model with no submodel accounting for chemistry change. Accounting for bath chemistry changes caused by freeze movement results in restrained solidification, and melting. For instance, at the end of the melting period, the ledge thickness decrease was 21.3 % lower, while the superheat increase was reduced by 33.8 %. However, the bath temperature rise was increased by 25.0 %. On the other hand, at the end of the solidification period, the ledge thickness increase was 25.6 % lower, while the reduction in superheat was 38.3 % lower despite a 17.1 % higher reduction in bath temperature. At the end of the melting and solidification periods, AlF_3 concentration changed by -12.5 % and +10.6 %, respectively, compared to the case with constant bath chemistry. The Python submodel paves the way for future enhancements of the full model by leveraging Python features unavailable in the commercial finite-element software.

Keywords: Transient thermoelectric model, Finite-element method (FEM), Bath chemistry, Mass transfer, Aluminium reduction cell.

1. Introduction

Aluminium is a metal with interesting thermo-mechanical properties – a good heat dissipator with a high mechanical strength-to-density ratio – that makes it suitable for use in many applications.

This metal is still being produced in the industry from its oxide through the conventional Hall-Héroult process in aluminium electrolysis cells (AEC) [1]:

$$2Al_2O_3 + 3C = 4Al + 3CO_2 \quad (1)$$

Alumina, a reactant in this process, is regularly fed to these cells where it dissolves in a cryolite-based electrolyte (Bath). Normal baths would mainly consist of cryolite (Na_3AlF_6), aluminium fluoride (AlF_3), calcium fluoride (CaF_2), and alumina (Al_2O_3) [2]. As the temperature in the vicinity of the side walls of the cell falls below the liquidus temperature of the bath, it freezes thus forming a solid called "the ledge". This ledge shields the cell lining from both physical and chemical degradation caused by the electrolytic bath and the liquid aluminium beneath it [3]. Thus, it is of utmost importance to ensure the existence of this layer and control its thickness [4] as failing to do so would result in a shortened cell life, which in turn would lead to unnecessary expenditure and increased residual materials [5]. This is especially important when the heat balance of the cell shifts, for instance, due to a power modulation. However, given the harsh conditions prevailing within electrolysis cells, measuring the evolving thickness and shape of the ledge using sensors immersed in the molten bath is extremely challenging if not altogether impractical [6]. To overcome this shortcoming, thermoelectric models of the AEC are widely used to predict the thermoelectric state of the cells and the ledge profile [3].

LeBreux et al. [6] introduced an online estimation tool to predict the evolving ledge profile in AECs by integrating thermal measurements with numerical simulations of the cell. Their results demonstrated that the tool could provide continuous and automated estimates of the ledge profile with an accuracy of ±2 cm, without the need for intrusive measurements or manual intervention by operators. Wong et al. [7] investigated the feasibility of power modulation and the resulting cell response using a spatially discretized dynamic material and energy balance model grounded in the principles of the thermodynamic laws. The results indicated that while a temporary change in power prevents the ledge from immediately returning to its original thickness, it gradually recovers over time. Moreover, repeated power modulation at relatively high frequencies may cause the average ledge thickness (during each consecutive melting and solidification phases) to converge to a constant value only after multiple cycles. Zhang et al. [8] developed a transient, strongly coupled thermoelectric model to investigate the dynamic behaviour of temperature distribution and heat dissipation in AECs under increased current conditions. Their results indicated that a current increase of up to 10 % over 2 hours caused minimal variation in the ledge profile. While the heat dissipation rate in the upper part of the cell (including the anode rod, steel stubs, and cover) changed, the percentage of change was lower than that of the other parts.

Allard et al. [9] developed an improved finite-element thermoelectric model of an AEC by measuring anode cover material (ACM) and anode crust profiles and their thermal conductivity and emissivity. Their model was also capable of predicting the cavity shape by utilizing a radiosity module coupled with an iterative method. Results indicated that increasing the ACM thickness decreases top heat losses and increases side heat dissipation while bottom losses stay unchanged leading to side ledge shrinkage and melting of the anode crust. In another study, Allard et al. [10] developed a new modelling approach to account for the displacements of solid bodies, e.g., anode, and moving boundaries, e.g., bath/ledge and crust/cavity interface, in finite element models which was demonstrated in a transient thermoelectric model of an AEC submitted to an increase in operating voltage. The simulation revealed that the anode cover deteriorates, and the side ledge thickness decreases in such a situation. It should be noted that the top heat dissipation remained higher (+1.4 % of the total dissipation), due to the ACM transformation into anode crust during the voltage increase, even after the operating voltage had been restored to its nominal value.

Lalancette et al. [5] proposed a new approach for online thermal diagnosis and process control, involving the development of a novel 2D model derived from an existing 3D slice model. Testing

of the model with some input currents in the range of 95 % to 105 % of the nominal current resulted in predictions for heat distribution that differed slightly (below 1 %) from the respective 3D model predictions. Furthermore, the ledge profiles were also found to be very similar with the largest difference being 1.8 cm. Pansiot et al. [11] introduced a new approach by incorporating a submodel into the cell half-slice model, aiming to reduce computation time. Their findings indicated that the computational time savings grew with greater deviations from the nominal state, reaching up to 70 % at certain time steps. A mathematical model, which consisted of material balance, cell voltage, and thermal balance models, was developed by Jessen [12] to simulate the transient behaviour of an aluminium reduction cell. Among others, their model could serve to predict the impact of changes in operating parameters on the cell's stability and performance. Additionally, it provides a basis for determining how much the operational parameters of the cell can be varied.

Despite all this, little attention has been paid to the consideration of bath chemistry variations in a 3D transient thermoelectric finite-element model of an AEC and the studies in the literature have at least one of the following shortcomings:

- Bath chemistry variation has been ignored.
- The effect of bath film, flowing between the metal and the ledge, on the bath chemistry is ignored.
- Lumped discretization is used.
- The pseudo-liquid method is used and convective thermal resistances at the bath/ledge and metal/ledge interface are ignored.
- The developed model is a steady-state model.

To resolve these shortcomings, this study has the following objectives and novelties:

- Development of a 3D transient thermoelectric finite-element model of an AEC by adapting an already-existing steady-state model;
- Adoption of a moving ledge approach (as opposed to the pseudo-liquid method), i.e., ledge and bath are defined as separate volumes that vary throughout the simulation;
- Definition of varying thermal contact conductances along the bath/ledge and metal/ledge interface to represent the convective thermal resistances between bath/metal and ledge;
- Development of a bath-chemistry submodel in Python with the possibility to be expanded in the future, and to couple it with the thermoelectric model;
- Consideration of the most important phenomenon affecting the bath chemistry in the submodel, i.e., phase change which includes latent heat;
- Simulation of a transient power modulation scenario with the developed model and its prediction analysis with and without the bath-chemistry submodel;
- Confirmation of the importance of considering bath-chemistry variations in a transient thermoelectric model of an AEC.

2. Methodology

In this study, a 3D steady-state thermoelectric slice model of an aluminium electrolysis cell representing the AP40 technology, which has been validated before – validation results were not published for this technology, but they were reported for the P155 technology in [9] – was adopted and modified to simulate transient scenarios. A similar steady-state model to the one used in this study was presented in [9] for another technology (P155). The model geometry, which is illustrated in Figure 1, is created by making one cut along the cell's length (at the centre) and two cuts along its width [10]. The AP40 slice model used in this study includes 1 half anode and 1 half cathode. A complete list of materials, representative of the real cell, with temperature-dependent thermophysical properties is defined and used in the model [5]. To account for the phase change of the materials used in the model – specifically the bath, ledge, and metal –

enthalpy has been simply defined as a function of temperature along with other thermophysical properties [6]. Furthermore, to avoid having to solve the fluid flow equations, the thermal conductivity of the bath and the metal layer underneath are boosted, i.e., an effective thermal conductivity k_{eff}, is used [5].

As for thermal boundary conditions, symmetry boundary conditions are applied on the cut surfaces [6]. Moreover, on the slice's top, side, and bottom, the Robin boundary condition has been applied to represent convective and radiative cooling [10]. Effective heat transfer coefficients (h_{eff}), including radiative effects, are used for different sections of the cell top, side, and bottom [10]. The following Equation (2) [10] is used to calculate these heat transfer coefficients, based on measurements taken beforehand for heat fluxes, surface temperatures, and ambient temperatures in the vicinity of the respective surfaces:

$$q'' = h_{eff} \cdot (T_s - T_\infty) \tag{2}$$

where:

q'' Heat flux, W/m^2
h_{eff} Effective heat transfer coefficient, W/m^2.°C
T_s Surface temperature, °C
T_∞ Ambient temperature, °C

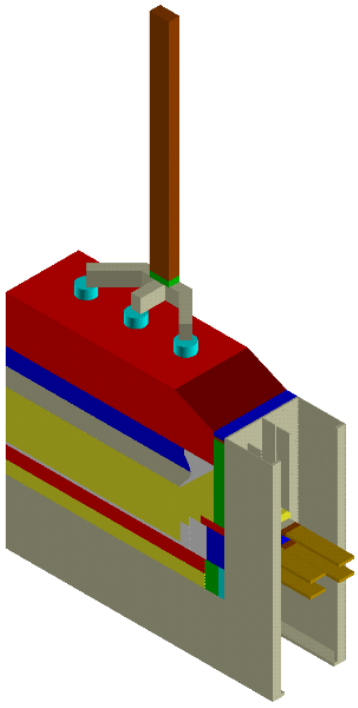

Figure 1. Geometry of the AEC slice model used in this study.

As for electrical boundary conditions, symmetry (insulating) boundary condition is applied on the cut surfaces [6]. Additionally, the total input current to the cell is divided by the number of anodes and the resulting value is applied to the top of the anode rod [10] (half anode current is used in this slice). Besides, a ground condition (0 V) is imposed on the end of each cathode flexible conductor [10].

Assumptions related to the slice model presented in [6] still hold for this study. However, this study removes the constant bath chemistry assumption, as investigating this effect is its primary objective. Additionally, unlike [6], modulation of the power input to the cell was achieved with variable input current to the cell.

A submodel was coded in Python to consider the effect of varying bath chemistry when cell thermal balance is disturbed. This submodel only considers the most important phenomenon that affects the bath chemistry, i.e., phase change. However, it can be expanded to include other physics related to bath chemistry. The upper ledge (i.e., the part facing the bath) forms through the solidification of the bath in front of it, which is primarily composed of cryolite. Thus, it was assumed that the upper ledge is made up of pure cryolite as in [7]. However, this assumption is not completely true and will be removed in our future study, which is currently underway. On the other hand, the lower ledge (i.e., the part facing the metal) forms from an alumina-saturated bath film that flows between the molten metal and this part of the ledge [13]. Accordingly, the lower ledge composition was assumed to follow eutectic corresponding to AlF_3 and CaF_2 concentrations of 3 % and 4 %, respectively [13, 14], which results in an alumina concentration of approximately 8.8 %. Moreover, it was assumed that the bath consists of four constituents, i.e., Na_3AlF_6, AlF_3, CaF_2, and Al_2O_3 [7]. The following system of differential equations was numerically solved by Python using the SciPy library:

$$\frac{dm_{AlF_3,b}}{dt} = -\dot{m}_{LFM} \times C_{AlF_3,eut} \tag{3}$$

$$\frac{dm_{CaF_2,b}}{dt} = -\dot{m}_{LFM} \times C_{CaF_2,eut} \tag{4}$$

$$\frac{dm_{Al_2O_3,b}}{dt} = -\dot{m}_{LFM} \times C_{Al_2O_3,eut} \tag{5}$$

$$\frac{dm_{Na_3AlF_6,b}}{dt} = -\dot{m}_{LFB} - \dot{m}_{LFM} \times C_{Na_3AlF_6,eut} \tag{6}$$

where:

$m_{X,b}$ Mass of bath constituent X, kg
$C_{X,eut}$ Eutectic concentration of bath constituent X in the lower ledge, fraction
$\dot{m}_{LFB}$ Mass variation rate of upper ledge, kg/s
$\dot{m}_{LFM}$ Mass variation rate of lower ledge, kg/s

In Equations 3–6, $\dot{m}_{LFB}$ and $\dot{m}_{LFM}$ are calculated as follows:

$$\dot{m}_{LFB} = \frac{\rho_{ledge} \times \Delta V_{LFB}}{\Delta t} \tag{7}$$

$$\dot{m}_{LFM} = \frac{\rho_{ledge} \times \Delta V_{LFM}}{\Delta t} \tag{8}$$

where:

ρ_{ledge} Ledge density, kg/m^3
ΔV_{LFB} Volume variation of the upper ledge, m^3
ΔV_{LFM} Volume variation of the lower ledge, m^3
Δt Time interval (time step), s

It is worth noting that in case of no phase change, both $\dot{m}_{LFB}$ and $\dot{m}_{LFM}$ would be equal to zero. Moreover, in the case of this study, Equations 3–6 can be solved as uncoupled algebraic equations.

However, if more physics were included in the submodel, this method could handle the potentially resulting system of coupled differential equations. This highlights the advantage of using Python alongside APDL. The flow diagram of the developed model is depicted in Figure 2.

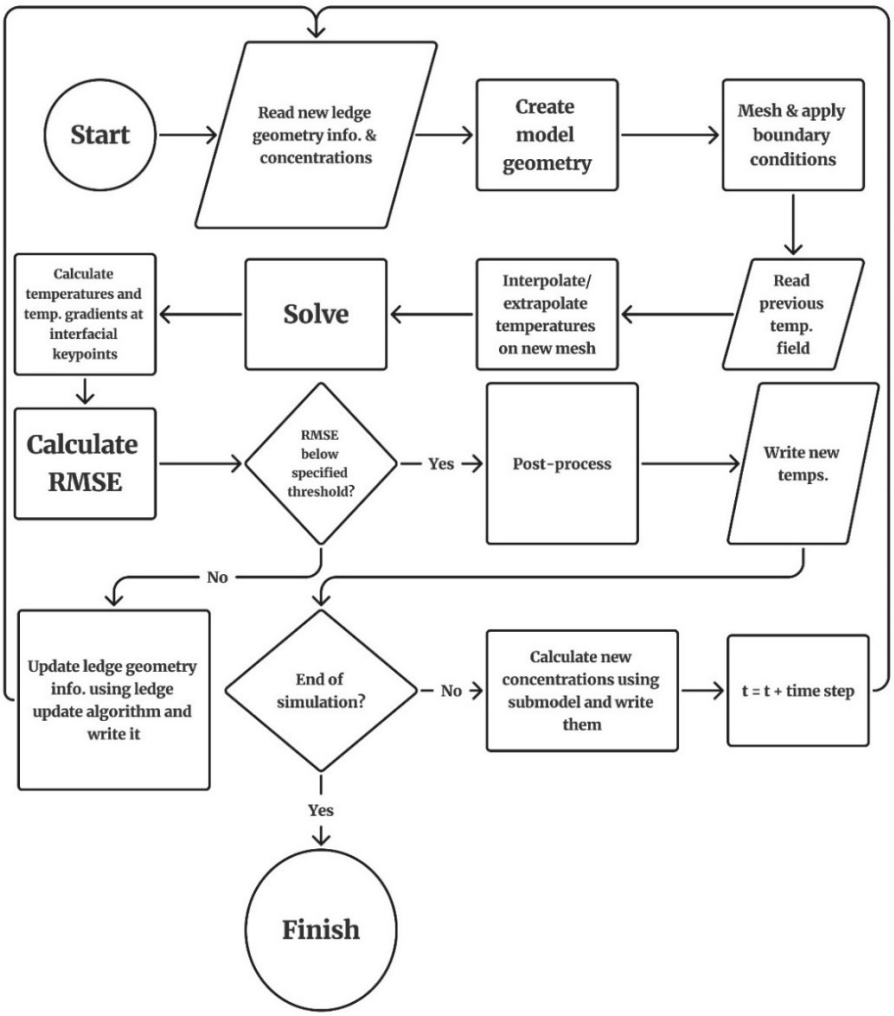

Figure 2. Flow diagram of the solution procedure of the developed transient model.

The model geometry is fully specified by the positions (x and y coordinates) of the key points that locate the bath/ledge and metal/ledge interface. Once the location of these points is read from the relevant file, ledge geometry is generated by creating a plane – by connecting these points and the key points on the ledge/cell side interface – and extruding it throughout the width of the model geometry. After this part of the geometry is created, the geometry of the bath and metal could be constructed. Since ledge geometry changes when cell heat balance is disturbed, model geometry changes accordingly at each time step. Thus, the model solution process is done one time step at a time, and during each time step, the geometry of the ledge is updated iteratively by a ledge update algorithm. That is, for one time step, the thermoelectric model solves the transient energy balance equations [6] using the finite-element method resulting in nodal solutions for both thermal and electrical fields. It has been assumed that mass transfer is controlled by heat transfer. Accordingly, in the next step, it is checked whether the interface is at bath liquidus temperature, i.e., if the root mean square of the temperature differences between the temperatures at the aforementioned key points and the liquidus temperature is below a predefined value. If this were not the case, the new interface position is predicted (by the ledge update algorithm), geometry is reconstructed, boundary conditions are reapplied, temperature field at the beginning of the time

step is interpolated/extrapolated on the new mesh (one material at a time), and eventually, the model is solved. This process continues until the interface is approximately at the liquidus temperature, which is verified by calculating the root mean square error (RMSE) as follows:

$$RMSE = \sqrt{\frac{\sum_{i=1}^{N}(T_i - T_{liq})^2}{N}} \quad (9)$$

where:

N Total number of key points on the bath/ledge and metal/ledge interfaces.
T_i Temperature at key point i, °C
T_{liq} Bath liquidus temperature, °C

Once this error is acceptable, post-processing of the nodal results is performed, through which various thermoelectric outputs, e.g., heat fluxes and voltage drops, are calculated and written to files. At this point, the solution procedure is deemed to be completed for one time step and the next timestep calculations start using the same described method. This procedure continues for as many time steps as needed to reach the end of the simulation time.

After the solution procedure for each time step has been completed, the volume of the upper and lower ledge and bath temperature are fed to the submodel as inputs which are then used to calculate the new concentrations for the next time step. As shown in Figure 2, concentrations of bath constituents, i.e., C_{AlF_3}, C_{CaF_2}, $C_{Al_2O_3}$, $C_{Na_3AlF_6}$, that are calculated by the submodel are fed to the slice model each time the solution procedure commences. These concentrations are used in the slice model to calculate liquidus temperature, bath thermophysical properties, and overvoltages.

3. Results and Discussion

To investigate the behaviour of the newly developed model, a power modulation scenario was considered as shown in Figure 3 (blue curve). It consists of two hours at nominal current followed by 12 hours at a boosted current of +10 % which is followed by 12 hours at a reduced power of -10 % (with respect to the nominal power), and finally another 12 hours at nominal power. This scenario was simulated using both the finite-element model coupled with the bath-chemistry submodel – referred to hereinafter as the variable-composition (VC) model – and the finite-element model without the bath-chemistry submodel – hereinafter called the fixed-composition (FC) model. A comparison of the average ledge thickness predictions of the VC and FC models is presented in Figure 3 (green and red curves respectively) for the considered scenario.

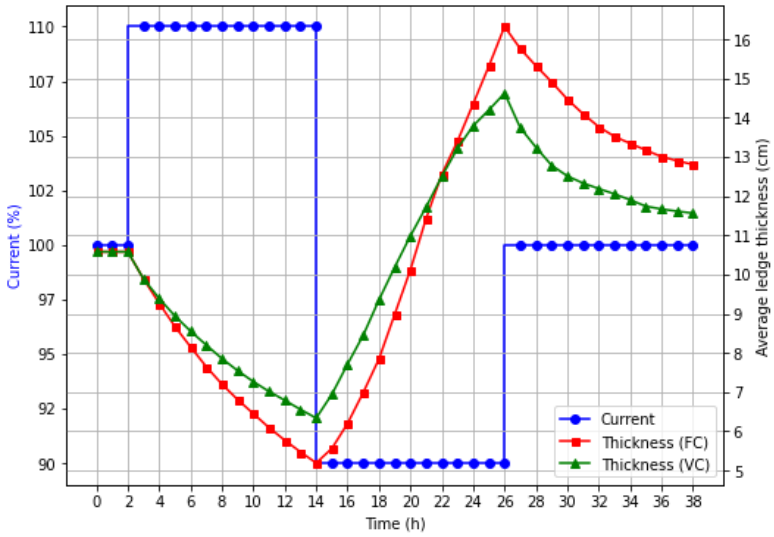

Figure 3. Simulated power modulation scenario and corresponding average ledge thickness variation predictions of the VC and FC models.

As illustrated in this figure, as the input power is boosted from t = 2 h, melting of the ledge starts and continues until t = 14 h, i.e., end of the power boost period. At this time, the predicted ledge thickness by the VC model is 22.0 % higher than that of the FC model. Melting of the ledge dilutes the bath by adding more cryolite to it which in turn increases its liquidus temperature. Since isotherms with higher temperatures are located toward the cell centre, the resulting ledge thickness prediction would be higher when the VC model is used. On the other hand, as the power is reduced from t = 14 h, the bath solidifies resulting in an increase in ledge thickness in both cases. However, the VC model predicts a 10.4 % thinner ledge at the end of the solidification period compared to the FC model. This could be explained by the fact that as the bath solidifies, the concentration of cryolite in the bath decreases resulting in a lower liquidus temperature. Accordingly, when the VC model is used, the ledge update algorithm will try to find an isotherm of lower temperatures which would be located towards the side of the cell resulting in a thinner ledge. Thus, considering the bath chemistry variations in a thermoelectric model of an AEC has the effect of restraining the phase change, be it solidification or melting. The comparison of the superheat variations during the simulated period has been depicted in Figure 4.

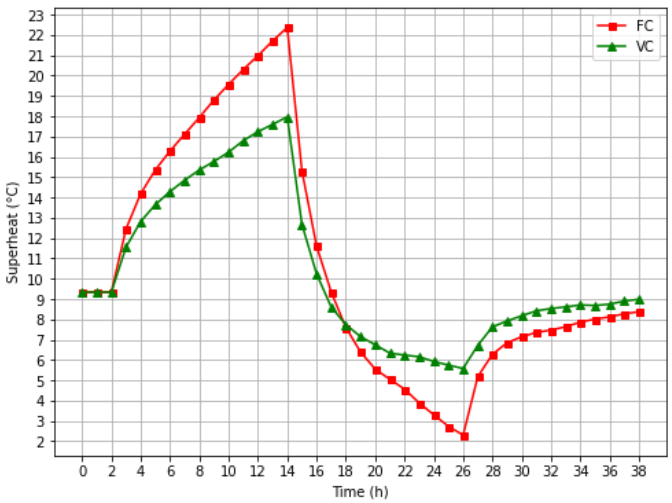

Figure 4. Comparison of superheat predictions of the VC and FC models for the considered scenario.

After the initial steady-state period (see the current profile in Figure 3), as the input power is increased at t = 2 h, superheat increases until t = 14 h after which it decreases until t = 26 h due to the decrease in the input power to the cell. Eventually, after t = 26 h, superheat increases as the current is restored to the nominal current from a level corresponding to 90 % of its initial value. At the end of the first melting period, i.e., t = 14 h, the VC model predicts a superheat that is 19.7 % lower compared to the FC model. To explain this, it should be recalled that superheat is defined as the difference between the bath temperature and the liquidus temperature of the bath. During this period, bath temperature increases due to the increase in power, and, in the VC model, liquidus temperature increases as well due to the dilution of the bath by cryolite. However, in the FC model, it is assumed that bath chemistry is constant resulting in a constant bath liquidus temperature. Considering the definition of superheat, higher figures will be predicted by the FC model for a period of power increase as the difference between the bath temperature and liquidus will be higher. On the other hand, at the end of the power decrease period, i.e., t = 26 h, a higher superheat is predicted with the VC model (142.4 % higher). This happens because when the input power of an AEC is decreased, the liquidus temperature of its bath decreases (as well as the bath temperature) due to the reduction in cryolite concentration of the bath. As this aspect is ignored in the FC model, the difference between the bath temperature and liquidus, i.e., superheat, would be lower.

In Figure 5, bath temperature predictions of the VC and FC models are compared. As illustrated in this figure, bath temperature increases during the two power increase periods, i.e., from t = 2 h to t = 14 h and from t = 26 h until the end, and decreases during the power decrease period, i.e., from t = 14 h to t = 26 h. It is interesting to note that although the VC model predicts a 3.3 °C higher bath temperature at t = 14 h, its predicted superheat is lower at this time (see Figure 4). On the other hand, although the two models predict a similar bath temperature at t = 26 h, the predicted superheat by the VC model is higher in the cooling period. Considering that superheat is an important parameter affecting the thermal balance of the cell, ignoring bath chemistry variations would have led to less precise predictions of this parameter among others. This highlights the importance of incorporating bath chemistry variations in AEC thermoelectric models.

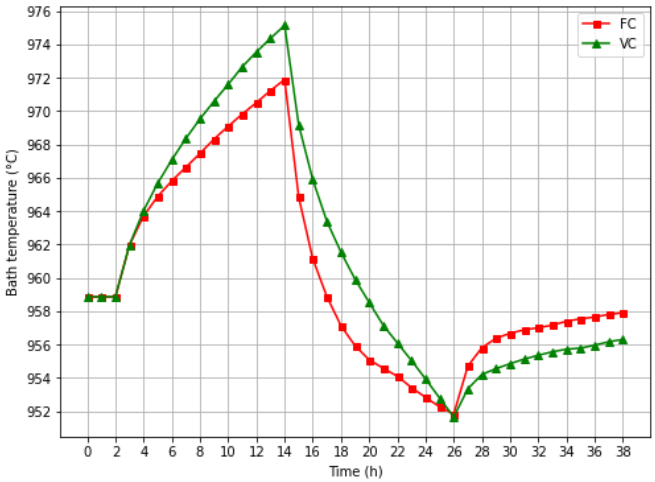

Figure 5. Comparison of bath temperature predictions of the VC and FC models for the considered scenario.

Maximum shell temperature predictions of the VC and FC models are shown in Figure 6. As observed in the figure, the maximum shell temperature prediction at the end of the power boost period, i.e., t = 14 h, is 5.7 °C lower for the VC model although its bath temperature prediction is

higher (see Figure 5). This stems from the fact that the ledge thickness predicted by the VC model is thicker at this time (see Figure 3) resulting in more insulation of the cell side from the hot bath as the thermal conductivity of the ledge is very low. However, this reasoning does not apply to the end of the power decrease period, i.e., t = 26 h. That is, although at this time ledge thickness predictions of the VC and FC models differ (see Figure 3) and bath temperatures are almost the same (see Figure 5), results show a similar maximum shell temperature. The reason for that could be that maximum shell temperature does not necessarily occur at the same height and the thermal resistance (ledge thickness) at two different heights could be similar for the VC and FC models. In other words, a difference in average ledge thickness for the VC and FC models does not necessarily translate to different local ledge thicknesses at each height. In addition, it should be noted that the maximum shell temperatures are not identical at t = 14 h for the two models, and the amplitude of variation is lower for the VC model during the solidification period, i.e., from t = 14 h to t = 26 h. Accordingly, the maximum shell temperature would have been higher for the VC model at t = 26 h if the maximum shell temperatures were identical at the beginning of the solidification period, i.e., t = 14 h.

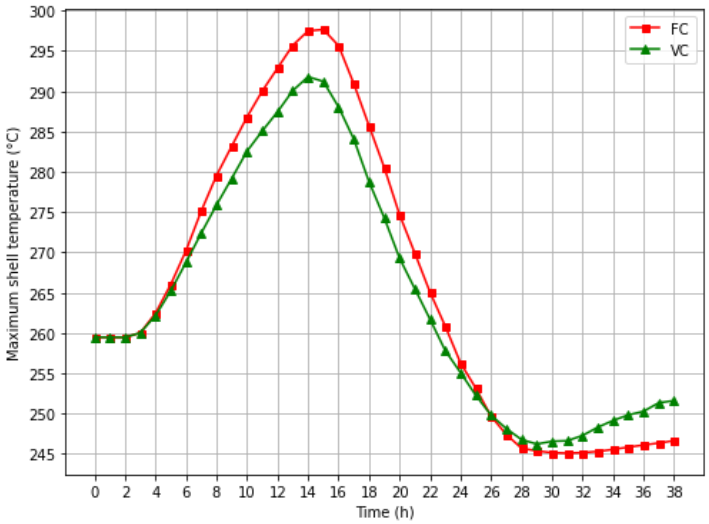

Figure 6. Comparison of maximum shell temperature predictions of the VC and FC models for the considered scenario.

As illustrated in Figure 7, incorporating bath chemistry variations through the VC model results in AlF_3 concentration changes of -12.5 % during the power boost period and +26.5 % during the power reduction period, relative to the values at t = 2 h and t = 14 h on the green curve, respectively. These changes are equivalent to liquidus temperature changes of +7.7 °C and -11.1 °C, respectively, in this case. These figures are by no means negligible and once again underscore the importance of accounting for bath chemistry variations in a finite-element thermoelectric model of an AEC.

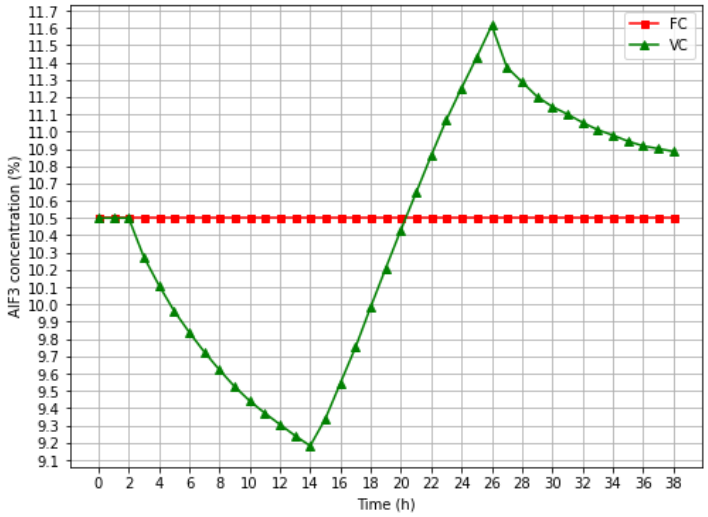

Figure 7. Effect of considering bath chemistry variations on AlF_3 concentration in the bath for the considered scenario.

Finally, ledge profiles at the beginning and end of the simulations for both the VC and FC models are illustrated in Figure 8. As evident in this figure, it was ensured that the steady-state ledge profiles (in dashed lines) were identical to ensure the same initial conditions for the VC and FC models. However, final ledge profile predictions of the VC and FC models are no longer identical at the end of the simulations and exhibit non-negligible differences. It is worth noting that at the end of the simulation time, i.e., t = 38 h, steady-state conditions have not been fully recovered for either of the models. This is because the thermal inertia is high and significantly more time is needed to return to the steady-state conditions. Ledge profile plays an important role in the heat balance of the cell as it substantially affects thermal resistance in the horizontal direction from the centre of the cell to its side. Accordingly, its evolution over the simulation time would affect the intermediate and final model predictions. Moreover, accurate ledge profile prediction is an important aspect of AEC thermoelectric models as cell life depends on the sustained presence of the ledge. Thus, the more precisely a model could predict it, the more valuable and reliable it would be. This is another proof that bath chemistry variations should be dealt with in transient thermoelectric models to achieve higher precision in ledge profile predictions.

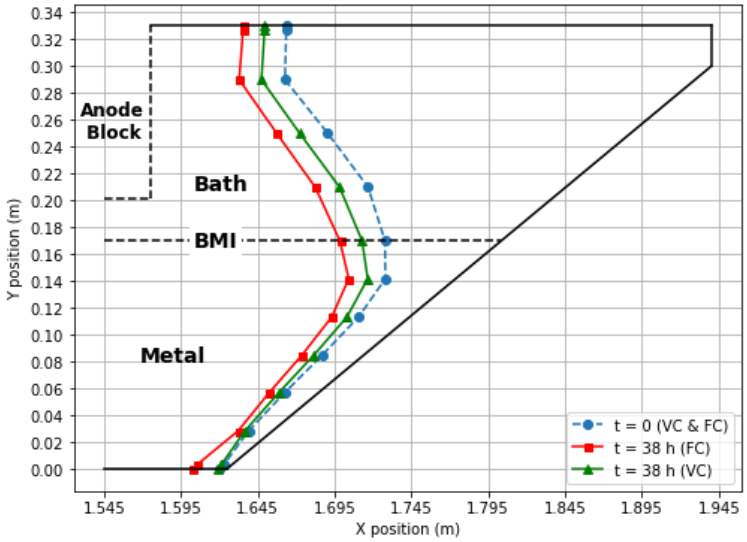

Figure 8. Initial and final predicted ledge profiles of the VC and FC models.

4. Conclusion

A 3D thermoelectric finite-element slice model of an AP40 AEC, which was originally developed to simulate the cell behaviour at a steady state, was modified to be applied to transient conditions. In this model, bath, and ledge were defined as two different volumes with different thermophysical properties. Moreover, the solution procedure consisted of an iterative solution for each time step. That is, at each timestep, until the bath/ledge and metal/ledge interfaces coincided with the bath liquidus isotherm, model geometry was recreated, boundary conditions were reapplied, the temperature field from the previous timestep was used as initial conditions for the current one, the model was resolved for the current time step, and the position of the interfaces was updated through a ledge update algorithm based on the solution results. This process was carried out for all time steps necessary to cover the full simulation duration. To consider the bath chemistry variations in such a model, a mass transfer submodel was coded in Python which considered the effect of bath phase change and the bath film flowing between metal and ledge on the electrolyte (bath) composition. A power modulation scenario was simulated with the developed model to demonstrate the capabilities of this model. It consisted of two hours at nominal current, 12 hours at 110 % of nominal current (first power boost period), 12 hours at 90 % of nominal current (power decrease period), and finally, 12 hours at nominal current (second power boost or recovery period) consecutively. Results were compared with the same model when the bath chemistry variations were ignored. The most important findings of this study are summarized as follows:

- When bath chemistry variations are considered, the average ledge thickness variations are 21.3 % and 25.6 % lower during the power boost and decrease periods, respectively. Accordingly, considering bath chemistry variations restrains the electrolyte phase change.
- The predicted superheat is 19.7 % lower and 142.4 % higher at the end of power boost and decrease periods, respectively, when bath chemistry variations are accounted for.
- When bath chemistry variations are considered, unlike superheat, the predicted bath temperature is 3.3 °C higher at the end of the power boost period while it does not change much at the end of the power decrease period.
- Accounting for bath chemistry variations results in a predicted maximum shell temperature that, unlike the bath temperature, is 5.7 °C lower at the end of the power boost period. However, similar to the bath temperature, it remains relatively unchanged at the end of the power decrease period.
- When bath chemistry variations are taken into account, AlF_3 concentration in the bath changes by -12.5 % and +26.5 % during the power boost and decrease periods, respectively, which corresponds to respective bath liquidus temperature changes of +7.7 °C and -11.1 °C in this case.
- Considering bath chemistry variations in a transient thermoelectric model of an AEC appreciably affects the thermoelectric states of the cell when the cell thermal balance has been disturbed resulting in different dynamic ledge profile predictions.

5. Acknowledgment

The authors gratefully acknowledge the financial support provided by Rio Tinto Aluminium, Mitacs, and the Natural Sciences and Engineering Research Council of Canada (NSERC). This work was made possible through their valuable partnership and collaboration. Furthermore, a part of the research presented in this paper was financed by the Fonds de recherche du Québec by the intermediary of the Aluminium Research Centre – REGAL.

6. References

1. Marc LeBreux et al., Modeling and measurements of anode cover behavior inside aluminium electrolysis cells, *Numerical Heat Transfer, Part A: Applications*, Vol. 69, No. 2, (2016), 128–145, https://doi.org/10.1080/10407782.2015.1069666
2. Jingjing Liu *et al.*, Investigation of the ledge structure in aluminium smelting cells, *JOM*, Vol. 72, (2020), 253–262, https://doi.org/10.1007/s11837-019-03863-4
3. Hongliang Zhang et al., Numerical investigation of flow field effect on ledge shape in aluminium reduction cell by coupled thermo-flow model, *Light Metals* 2020, 517–526, https://doi.org/10.1007/978-3-030-36408-3_72
4. Jingjing Liu et al., Investigation of the influence of heat balance shifts on the freeze microstructure and composition in aluminium smelting bath system: Cryolite-CaF2-AlF3-Al2O3, *Metall and Mat Trans B*, Vol. 48, No. 6, (2017), 3185–3195, https://doi.org/10.1007/s11663-017-1109-3
5. Francis Lalancette et al., Dimensional reduction of a 3D thermoelectric model to create a reliable and time-efficient 2D model representing an aluminium electrolysis cell, *International Journal of Heat and Mass Transfer*, Vol. 202, (2023), 123777, https://doi.org/10.1016/j.ijheatmasstransfer.2022.123777
6. Marc LeBreux et al., An on-line estimation tool for predicting the time-varying ledge profile inside aluminium electrolysis cells, *Numerical Heat Transfer, Part A: Applications*, Vol. 77, No. 2, (2020), 134–161, https://doi.org/10.1080/10407782.2019.1687201
7. Choon-Jie Wong *et al.*, Studies on power modulation of aluminium smelting cells based on a discretized mass and thermal dynamic model, *Metallurgical and Materials Transactions B*, (2023), 1–16, https://doi.org/10.1007/s11663-022-02709-w
8. Hongliang Zhang et al., Effect of current transient enhancement on thermal field of aluminium electrolysis cell for the accommodation of wind power, *Journal of Sustainable Metallurgy*, Vol. 4, No. 3, (2018), 359–366, https://doi.org/10.1007/s40831-018-0177-1
9. François Allard et al., Improved heat transfer modeling of the top of aluminium electrolysis cells, *International Journal of Heat and Mass Transfer*, Vol. 132, (2019), 1262–1276, https://doi.org/10.1016/j.ijheatmasstransfer.2018.12.062
10. François Allard, Martin Désilets, and Alexandre Blais, A modeling approach for time-dependent geometry applied to transient heat transfer of aluminium electrolysis cells, *Metallurgical and Materials Transactions B*, Vol. 50, No. 2, (2019), 958–980, https://doi.org/10.1007/s11663-019-01510-6
11. Bastien Pansiot et al., Optimizing power modulation simulation in aluminium electrolysis cells: a sub-modeling approach for thermal-electrical analysis, Submitted.
12. Stefan Winkel Jessen, *Mathematical modeling of a Hall Héroult aluminium reduction cell*, MSc Thesis, Technical University of Denmark, Kongens Lyngby, Denmark, 2008.
13. Asbjørn Solheim, Nils-Håvard Giskeødegård, and Nancy J. Holt, Sideledge facing metal in aluminium electrolysis cells: Freezing and melting in the presence of a bath film, *Light Metals* 2016, 333–338, https://doi.org/10.1002/9781119274780.ch55
14. Asbjørn Solheim et al., Sideledge in aluminium cells: Further considerations concerning the trench at the metal-bath boundary, *Light Metals* 2019, 787–793, https://doi.org/10.1007/978-3-030-05864-7_96